

The transformation of U(VI) and V(V) in carnotite group minerals during dissimilatory respiration by a metal reducing bacterium

Susan Glasauer^{a,*}, Sirine C. Fakra^b, Sarah Schooling^a, Peter Weidler^c, Tolek Tyliczszak^d, David K. Shuh^d

^a School of Environmental Sciences, University of Guelph, Guelph, ON N1G 2W1, Canada

^b Advanced Light Source, Lawrence Berkeley National Laboratory, Berkeley, CA 94720, USA

^c Institute of Functional Interfaces, Karlsruhe Institute of Technology, Karlsruhe, Germany

^d Chemical Sciences Division, Lawrence Berkeley National Laboratory, Berkeley, CA 94720, USA

ARTICLE INFO

Editor: Dr. Hailiang Dong

Keywords:

Metal reduction

Shewanella

Carnotite

Uranium

Vanadium

Scanning transmission X-ray microscopy

ABSTRACT

Recent results from laboratory and field studies support that dissimilatory metal reducing (DMR) bacteria influence the fate and transport of uranium in anaerobic subsurface environments. To date, most research efforts have focused on the reduction of soluble U(VI) by DMR bacteria to form insoluble uraninite (UO₂). Subsurface environments harbor, however, large reservoirs of U(VI) in solid or mineral form. Uranium that is structure-bound in minerals is expected to be more refractory to microbial reduction than soluble U, based on analogy with Fe respiration. The reducibility of U(VI) could impact the fate of U(IV) by controlling mineral precipitation reactions, which has implications for the long-term immobilization of U in subsurface environments. We studied anoxic cultures of *Shewanella putrefaciens* CN32 incubated with natural carnotite-group minerals by X-ray diffraction, electron microscopy, scanning transmission X-ray microscopy (STXM). Near-edge X-ray absorption fine structure (NEXAFS) spectroscopy measurements at U-N_{4,5}, V-L_{2,3}, and O-K edges on cultures incubated up to 10 months show that V(V) was reduced to V(IV), whereas U was not reduced. In contrast, V(V) and U(VI) in solution were both completely reduced to lower oxidation states by CN32, as precipitates within the exopolymer surrounding the bacteria. Assays for the toxicity of U and V to CN32 showed that biofilm formation was stimulated at 0.001 M U(VI), and growth was inhibited at concentrations of U(VI) greater than 0.001 M. Vanadium did not inhibit growth or stimulate biofilm formation at any concentration tested. Investigations of the bacteria-mineral and bacteria-metal interface at the nanometer and molecular scales provide new insights into the co-respiration of V and U that help explain their biogeochemical cycling and have implications for subsurface bioremediation of these elements.

1. Introduction

The most important ore minerals of the Colorado Plateau uranium deposits belong to the uranyl vanadate group, also known as carnotite group minerals (CGM). These include carnotite [K₂(UO₂)₂(V₂O₈)(H₂O)₃] and tyuyamunite [Ca(UO₂)₂(V₂O₈)(H₂O)₈], which consist of uranyl divanadate (V₂O₈)⁶⁻ layer complexes that are analogous to layer silicates and contain cations in the interlayer positions (Evans and White, 1987). The ability of uranyl vanadate minerals to accommodate different interlayer cations explains the wide range of possible compositions (Evans and Garrels, 1958; Evans and White, 1987; Finch and Murakami, 1999). The Colorado Plateau ores were processed for

radium, vanadium and uranium since the late 19th century (Thews and Heinle, 1923; Weeks, 1961), leaving legacies of tailings. Although they are considered insoluble under the slightly alkaline, oxidizing conditions that dominate Colorado Plateau surface environments today (Evans and Garrels, 1958; Langmuir, 1978), extraction activity has resulted in areas of elevated concentrations in Utah and Colorado as well as in other locations where U was processed.

The reduction of soluble U(VI) by some bacteria is well documented (e.g., Lovley et al., 1991; Haas and DiChristina, 2002; Lloyd et al., 2002; Lloyd and Renshaw, 2005; reviewed in Kolhe et al., 2018). Bioremediation strategies that center on manipulating the activities of dissimilatory metal reducing (DMR) bacteria have been explored for the removal

* Corresponding author.

E-mail address: glasauer@uoguelph.ca (S. Glasauer).

of U(VI) from groundwater, perhaps most notably at Rifle, CO (e.g., Xu et al., 2017; Bargar et al., 2013; Williams et al., 2011; Zhuang et al., 2012; Li et al., 2010; Vrionis et al., 2005; Ortiz-Bernad et al., 2004b; Anderson et al., 2003). Subsurface bioremediation strategies are based on the reduction of U(VI) species to relatively insoluble hydroxylated uranate complexes (Langmuir, 1978; Bargar et al., 2013; Stylo et al., 2013). In contrast to studies with soluble U(VI), the ability of DMR bacteria to reduce U(VI) that is present in natural minerals has received less attention. This is a striking gap in the understanding of how bacteria may transform U, given that solid mineral phases are the largest reservoirs of metals in weathering environments, as well as the ultimate sinks. Several synthetic U(VI) mineral analogs have been shown to be reducible by dissimilatory bacteria, including: metaschoepite [UO₃·2H₂O] (Fredrickson et al., 2000), uramphite [(NH₄)(UO₂)(PO₄)·H₂O] (Khijniak et al., 2005), synthetic U(VI) borate and boronate crystals (Yang et al., 2014), and natural boltwoodite [HK(UO₂)(SiO₄)·H₂O] (Liu et al., 2006; Liu et al., 2009). In one study, the U(VI) contained in meta-autunite (Ca[(UO₂)(PO₄)](H₂O)₆) could not be reduced by DMR bacteria (Smeaton et al., 2008). The U(VI) minerals in these studies are, however, much less widespread than for CGM, which are associated with roll front deposits in the Colorado Plateau and in Australia (reviewed in Cumberland et al., 2016).

The V(V) contained in CGM is another possible electron acceptor. Given its favorable solution and redox chemistry (Wehrli and Stumm, 1989; Huang et al., 2015), vanadium should compete effectively with U(VI) for electrons produced during respiration by DMR bacteria. The aqueous chemistry of vanadium is complex due to multiple oxidation states and strong tendencies to hydrolyze and polymerize (Macara, 1980; Rehder, 2008). Vanadate ions (H₂VO₄⁻ and HVO₄⁻) are relatively stable under oxidizing conditions, exhibiting chemical behavior similar to phosphate. Vanadyl (VO²⁺) species are found in reducing environments and are typically more insoluble than vanadate ions (Eckstrom et al., 1983; Premovic et al., 1986). Trivalent V occurs in complexes of low solubility under strongly reducing, i.e., sulfidic, conditions (Wehrli and Stumm, 1989). Several bacterial species have been shown to reduce soluble V(V) to V(IV), including *Shewanella oneidensis* and *Geobacter metallireducens* (Lyalikova and Yurkova, 1992; Carpentier et al., 2003, 2005; Ortiz-Bernad et al., 2004a), as well as a native microbial community (Hao et al., 2018). There is just one report of reduction to V(III) (Li et al., 2007). To the best of our knowledge, the bacterial reduction of solid or mineral-bound V has not been investigated.

Bacteria introduce complexity to geochemical reactions by their ability to establish micro and nanoscale chemical gradients (Hunter and Beveridge, 2005). To investigate the bioreactivity of mineral U and V, we incubated anoxic cultures of *Shewanella putrefaciens* CN32 with natural CGM contained in U ore associated with sandstone and examined the products using nanoscale synchrotron-based X-ray spectromicroscopy techniques. *S. putrefaciens* CN32 is known to reduce U as well as Fe and other transition metals (reviewed in DiChristina et al., 2005). Because CN32 was originally isolated from Colorado Plateau deposits, it is a relevant model organism for investigating biological contributions to the terrestrial cycling of metals in this environment.

Our investigations were centered on testing: 1) whether the presence of V(V), an alternate electron acceptor, will inhibit the reduction of U(VI) by DMR bacteria; 2) whether the chemical phase of U and V, i.e., solid vs. soluble, will affect bacterial dissimilatory reduction and associated mineral products, and 3) bacterial growth responses to U and V. To characterize the samples, we used soft X-ray scanning transmission X-ray microscopy (STXM), electron microscopy, X-ray diffraction and wet chemical techniques. Elemental mapping (C, K, Ca, O, Mn, Fe, V, U and Ba) and NEXAFS spectroscopy at U 4f, V 2p and O1s edges were performed using STXM on minerals and bacteria samples over the 10-month incubation period, in both dry and hydrated sample conditions. The combination of bulk analyses with spectromicroscopic techniques at the nanoscale allowed us to capture the small-scale heterogeneity induced by active bacteria as well as the relative magnitude of the observed

changes in mineralogy.

2. Materials and methods

2.1. Materials

Material from a stockpile of unprocessed uranium ore was obtained from southeastern Utah, where it is associated with roll front and tabular deposits of the Colorado Plateau (Weeks, 1961; Finch and Murakami, 1999). The uranium minerals occur as coatings on consolidated sandstone that is porous and friable, which we identified using XRD. The metal concentrations of solids were determined using an adaptation of EPA SW 846 Method 3050B. The mineral sample (between 10 and 40 mg) was digested with three ml of HCl and 1 ml concentrated HNO₃ (trace metal grade) in a Teflon bomb overnight followed by 110 °C for 3 h in an oven. The sample was filtered (Whatman #42) and diluted to 50 ml with deionized water, followed by analysis using inductively coupled plasma spectroscopy (ICP-OES; Varian Vista Pro) or atomic absorption spectroscopy with graphite furnace (Varian GTA100Z). All mineral assays were performed in triplicate and replicates had standard deviations of 5% or less. The mineral-coated sandstone contained 14.6 g V kg⁻¹ and 111 g U kg⁻¹. In order to obtain a concentrated sample of the U-bearing minerals for XRD, the fine mineral fraction was separated from the sand grains by agitating and sonicating in deionized water; decanting, centrifuging and drying the separated fine minerals. These were digested and analyzed as described above and characterized also by XRD and SEM-EDS to identify the minerals.

2.2. Culture experiments

2.2.1. Cultivation of CN32 with U and V as electron acceptors

The cultures of *S. putrefaciens* CN32 that we used were originally isolated from the Morrison Formation in New Mexico (Fredrickson et al., 1998). It is, therefore, a terrestrial rather than a marine isolate and occurs in the same geological setting as the U-ore minerals. Cultures were maintained as frozen stocks in our lab and were revived from frozen stock for each experiment. The defined culture medium (DM) contained 10 mM sodium lactate and 1 mM phosphate, added as Na₂HPO₄, as previously described in Glasauer et al., 2003. Cultures reached the stationary growth phase under oxic conditions after around 24 h. For the incubation experiments with the U-ore, 1.6 g of CGM-sandstone was added to 80 ml of minimal medium + lactate in serum bottles, degassed with N₂, sealed and autoclaved. Bottles were inoculated in the glove box (Coy; 3% H₂/97% Ar) where they remained throughout the experiments. For the treatments with soluble U and V, preparation and incubation conditions were identical, except U and V were added from stock solutions prepared from uranyl acetate and sodium vanadate, respectively. Final concentrations for U and V for these treatments were 1 mM each.

CN32 cultures were prepared for inoculation as previously described (Glasauer et al., 2003). After conditioning the bacteria to grow on the defined medium (DM), the final pellet was resuspended in DM to form a slurry of bacteria. The slurry was transferred to the glove box (no-vacuum mode) and inoculated to achieve an initial concentration of around 10⁸ cfu ml⁻¹, determined by protein assay (Glasauer et al., 2001). All treatments were performed in triplicate.

2.2.2. Growth inhibition assay

For the growth inhibition assay, we selected conditions to model exposure of bacteria to U(VI) and V(IV), the oxidation states of U and V that dominated in the incubation treatments with CGM. Conditions were oxic to maintain the oxidation state of the metals and to facilitate the assay procedures. A modified micro-dilution method (Wiegand et al., 2008) was used to assess soluble U(VI) and V(IV) (0.001–1 mM) for microbial growth inhibition. In order to compare the response of CN32 to *E. coli* K-12, a well characterized bacterial strain, bacteria were

cultured in one-tenth strength trypticase soy broth (10% TSB) that has been shown to be compatible with metal and mineral studies (French et al., 2013a; Hunter and Beveridge, 2005). The volume was set to 200 μ l/well. Stock solutions containing 0.02 M $\text{UO}_2(\text{CH}_3\text{COOH})_2$, 0.1 M VCl_4 , or 0.1 M CaCl_2 were deoxygenated by bubbling oxygen-scrubbed N_2 gas (30 min/100 ml and 10 min for headspace degassing). VCl_4 was prepared in HCl and solutions were pH-adjusted with NaOH. Degassed solutions were transferred to an anaerobic chamber and sterilized by syringe filtration through a sterile 0.22 μ m filter into acid-washed autoclaved serum bottles. The stock solutions were removed from the anaerobic chamber, stored in the dark, and visually inspected for precipitates, flocs or colour change prior to use. Aliquots were aseptically removed from the stock solutions, as required, using a syringe and fine gauge needle. *S. putrefaciens* CN32 and *E. coli* K-12 were inoculated into 10% TSB and grown for 16–20 h (room temperature, 60 rpm). 10% TSB was inoculated from these starter cultures at 15% (vol/vol); stirred at 300 rpm (stir plate) at room temperature (*S. putrefaciens* CN32) or 37 °C (*E. coli* K-12), grown to an OD_{600} of 0.4–0.5 units and adjusted to a final in-assay concentration of 5×10^5 CFU/ml. Negative growth control wells contained sterile medium; positive growth control wells contained inoculated medium. The plates were incubated for 20 h at optimum conditions (room temperature for *S. putrefaciens* CN32 or 37 °C for *E. coli* K-12), then removed and observations on the presence/absence of visible growth were recorded. The MIC was the lowest concentration which resulted in optically clear wells denoting no cell growth. Assays were done as triplicate replicates and repeated as independent duplicate experiments ($n = 6$).

2.2.3. Biofilm formation assay

The influence of soluble U(VI) and V(IV) (0.001–1 mM) on biofilm formation was performed as for the growth inhibition assay except that the biofilms were grown on the inner wall of sterile glass tubes which contained 2 ml volumes of 10% TSB with U, V or Ca added. Following incubation for 20 h at room temperature (*S. putrefaciens* CN32) or 37 °C (*E. coli* K-12), the tubes were removed and 0.1 ml of Hucker's crystal violet was added. After 15 min incubation (room temperature), the contents were gently decanted, excess unretained stain was removed by washing with distilled water, and the tubes were air dried. Retained stain was solubilized with 33% acetic acid and the absorbance (600 nm) was measured using a Bio-Tek EL800 plate reader. Assays were done as triplicate replicates and repeated as independent duplicate experiments ($n = 6$).

2.3. Assessment for biotransformed elements

2.3.1. Electron microscopy

Samples for transmission electron microscopy (TEM) were prepared as previously described, for whole mount and thin section preparation (Glasauer et al., 2001). No metal stains were used, so that all observed contrast was imparted to the bacteria by the metals (chiefly U and V) present in the culture medium. Observations were made using a Philips CM10 TEM operating at 80 kV, using an EDAX Sapphire detector and Genesis software. Scanning electron microscopy was performed on untreated CGM-ore, and after 4 months incubation with CN32 on a Hitachi S4500 field emission SEM. Secondary electron (SE) images were obtained with a 5 kV electron beam. The samples were sputtered with gold to alleviate charging problems during SEM examination.

2.3.2. X-ray diffraction

Biotransformation of the CGM appeared to have ceased by 10 months. At this time, the mineral solids were separated into their component fractions, identified as the sand or fine fraction. Separation was carried out in the glove box (3% H_2 /97% Ar). Suspensions were shaken and the suspension bearing the fine clay fraction was decanted. This process was repeated until the wash solution remained clear. All washes were combined in one centrifuge tube, which was sealed,

removed from the glove box, and centrifuged (5000 xg). The resulting pellet was dried in the glove box and lightly crushed with a mortar for analysis.

XRD data were acquired with a custom X-ray diffractometer at the Department of Physics, University of Guelph. The X-ray diffractograms were recorded from 5 to 80° 2θ with a step width of 0.0125° 2θ and five seconds counting time. The applied Cu wavelength was created by a rotating anode. Analysis of the XRD data was carried with the help of the evaluation program EVA15.0 and LeBail (Le Bail et al., 1988) with TOPAS4–2 by Bruker AXS.

2.3.3. Scanning Transmission X-ray Microscopy (STXM)

STXM analyses were conducted at the Molecular Environmental Science Beamline 11.0.2 (90–2000 eV) of the Advanced Light Source at Lawrence Berkeley National Laboratory (Bluhm et al., 2006). Culture samples were enclosed between a pair of 100 nm thick Si_3N_4 membranes. A micro-liter droplet of culture was deposited onto a Si_3N_4 window (Silson Ltd.), air-dried and then sandwiched with another window and hermetically sealed with glue. Another batch of treatments were analyzed in hydrated conditions using the same protocol, except the wet droplet was sandwiched immediately and the assembly sealed with glue. Uranium-bearing powder standards were deposited onto a Si_3N_4 window using a standard inspection microscope at 20 \times magnification. A 2 cm human hair fiber fixed to a tantalum wire was used to transfer the radioactive powder particles onto the window, then sandwiched and hermetically sealed with glue. Standards measured were $^{238}\text{UO}_2$ obtained from Alfa-Aesar, and mineral samples were obtained from Excalibur Mineral Corporation (New York). Small metal foil containers were inserted into the STXM prior to use with radioactive materials so that radioactive material could be captured in case of membrane failure.

STXM measurements were performed using a Fresnel zone plate lens (35 nm outer zones) to focus a monochromatic X-ray beam onto a 2D-scanned sample to record images in transmission mode using a scintillator-photomultiplier detector assembly. The imaging contrast is based on core electron excitation by X-ray absorption. X-ray images recorded at energies just below and at the relevant absorption edges were converted into optical density (OD) images and used to derive elemental maps. The optical density (OD) can be expressed for a given X-ray energy by the Beer-Lambert law as $\text{OD} = -\ln(I/I_0) = \mu \rho t$ where I is the transmitted flux through the sample, I_0 is the incident flux, μ is the mass absorption coefficient, ρ is the density and t is the sample thickness. NEXAFS measurements were performed at the V 2p, O 1 s and U 4f edges and obtained from image sequences (i.e., stacks) collected at energies spanning the relevant element absorption edges (508–555 eV at V 2p, O 1 s edges; 715–800 eV at U 4f edges, unless otherwise specified). A minimum of two different sample regions were analyzed for each element and two different batches of samples were analyzed. Radiation beam-induced damage was not observed over the course of measurements of dry samples, but cannot be ruled out on the wet samples at the V L2,3 and O K-edges. The STXM was pumped-purged with He to avoid decompressing the Si_3N_4 sandwiched samples. The theoretical spectral and spatial resolutions during our measurements were ± 100 meV and 40 nm respectively. The photon energy was calibrated at the C 1 s edge using the 3p Rydberg peak of gaseous CO_2 at 292.74 eV, at the O1s using the O 1 s \rightarrow 3 s transition at 538.9 eV of gaseous CO_2 and at the U 4f edges using gaseous Neon transition at 867.3 eV. All data processing was carried out using IDL aXis2000 software (Hitchcock, 2019).

3. Results

3.1. Characterization of the sandstone ore minerals

The U- and V- containing mineral components occurred as bright yellow coatings of fine basal plates (1–2 μ m) on sand grains (grain size 200–500 μ m) (Fig. 1). The U-coated sandstone contained around 11% U

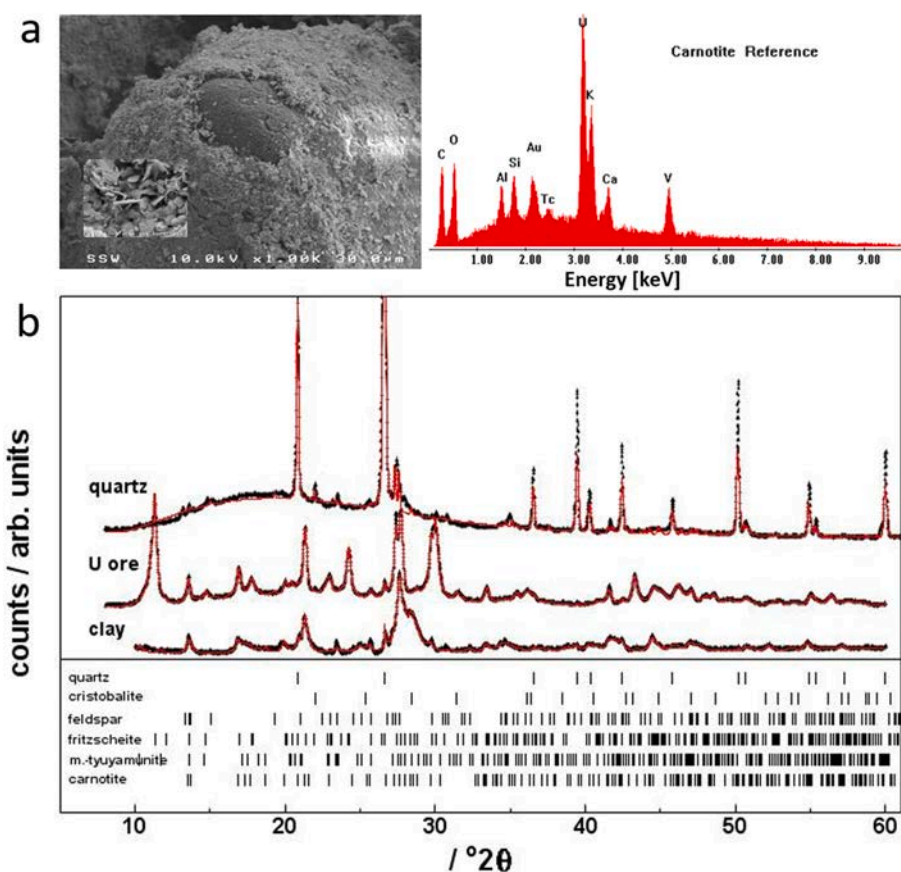


Fig. 1. a) Grain of quartz sand coated with U- and V-containing minerals observed by scanning electron microscopy and energy dispersive spectroscopy b) X-ray diffractograms of the separated sand (upper), fine yellow U-containing solids (tyuyamunite; middle) and fine clay material separated after incubation with *Shewanella putrefaciens* CN32. Continuous lines represent results of whole pattern fitting. (For interpretation of the references to colour in this figure legend, the reader is referred to the web version of this article.)

and 1.5% V by weight. Based on the fit of the diffraction peaks, the space group, and the chemical composition of the separated fine fraction (Table 1), we identified the main minerals of the yellow solid as meta-tyuyamunite $[\text{Ca}(\text{UO}_2)_2(\text{V}_2\text{O}_8)\cdot 3\text{H}_2\text{O}]$ and fritzscheite $[\text{Mn}(\text{UO}_2)_2(\text{V}_2\text{O}_8)\cdot \text{H}_2\text{O}]$ (Finch and Murakami, 1999) (Fig. 1). Both minerals are members of CGM, which consist of uranyl divanadate layer complexes with interlayer cations. The space group for both minerals is orthorhombic as confirmed by applying the LeBail method (Le Bail et al., 1988). Meta-tyuyamunite is a dehydrated variant of tyuyamunite and can accommodate up to several percent structural K (Stern et al., 1956). Barium can substitute for Mn in the interlayer of fritzscheite, but the structure does not accommodate K (Finch and Murakami, 1999). Chemical analysis revealed that both Ba and Mn are present in the fine fraction of the CGM ore (Table 1) as also confirmed by STXM (Appendix A).

Table 1

Element concentrations for separated fine yellow particles of uranium ore and fine mineral fraction after incubation with *Shewanella putrefaciens*. The standard deviation for. triplicate samples was less than 5%.

Element	U-ore, mg/kg	Incubated U-ore, mg/kg
U	301,384	293,880
V	73,458	66,615
Na	134	1805
K	832	4402
Ca	19,940	5440
Mg	1296	1669
Ba	1778	1498
Fe	3930	5145
Mn	3643	3303

3.2. Microbial reduction of V and U

Each incubation treatment with the CGM contained a total of 5 mM V and 7 mM U. Total soluble V initially increased, followed by a decrease to a plateau at around 1 mM by 120 days (Fig. 2). The concentration of dissolved uranium was low throughout the incubation.

Vanadium III, IV, and V may be visually differentiated in solution by green, blue and orange/yellow colors, respectively (Macara, 1980; Evans and White, 1987). The treatments that contained the CGM ore and CN32 developed a blue-green colour within one hour of inoculation. Over time, the characteristic bright yellow colour of the CGM disappeared. We observed the development of three distinct layers in the culture bottles: clean sand grains at the bottom, a layer of grey-green fine material, and clear blue liquid. Analysis for total U and V in the fine fraction showed no change in U concentration after 10 months, and a slight decrease in V (Table 1). The alkali elements Na and K were higher in the fine fraction after incubation, which likely reflects the Na and K present in the culture medium. Calcium was significantly lower, Mg showed little change, and Ba was slightly decreased in the post-reduction solids. The increase in K and decrease in Ca of the solids is consistent with the observed transformation from tyuyamunite to carnotite $[\text{K}_2(\text{UO}_2)_2(\text{V}_2\text{O}_8)\cdot 3\text{H}_2\text{O}]$.

Bacteria were still viable after 5 months at a density of around 5×10^5 colony forming units (cfu) ml^{-1} . The population reached a plateau around 10^5 cfu ml^{-1} that was maintained between 6 d and at least 138 d. The cell density was around 10^3 cfu ml^{-1} after 8 months. Cell numbers could be underestimated due to the tendency of the bacteria to form flocs; other methods for determining cell numbers (i.e., fluorescent probes, light scattering) could not be used due to the interference of the minerals with light. Bacteria were closely associated with the mineral particles throughout the incubation (Fig. 3). Over time, biofilms with cells embedded in a matrix of exopolymeric substances (EPS) decreased

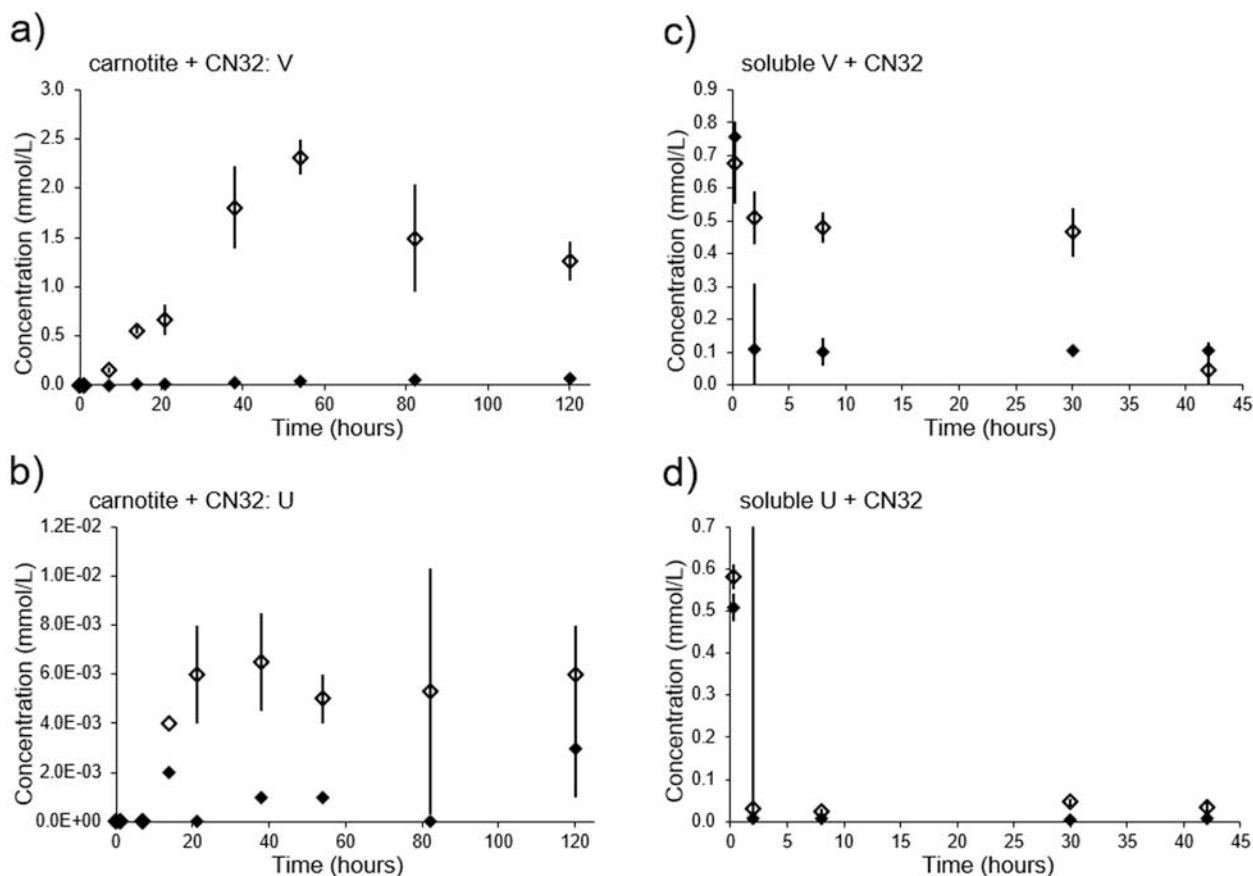


Fig. 2. Changes in solution concentrations of V and U. Concentrations of dissolved vanadium (a) and uranium (b) during anaerobic respiration of *Shewanella putrefaciens* CN32 in the presence of carnotite. Concentrations of dissolved vanadium (c) and uranium (d) during incubation with a mixed solution containing soluble V(V) and U(VI) at 1 mM concentrations. Open diamonds represent treatments inoculated with CN32; filled diamonds are bacteria-free control treatments.

in abundance, and bacteria were observed mainly as single or few cells by four months (Fig. 3 and Appendix B).

For comparison with the CGM treatments, we inoculated anoxic media containing dissolved V(V) and U(VI) at 1 mM concentration each with CN32 cultures. These concentrations are below the minimal inhibitory concentrations (MIC) of V(V) and U(VI) for *E. coli*, a Gram-negative model bacterium (Nies, 2007); MIC data for CN32 is not available. The cultures were monitored for V, U and cell concentrations for one week, at which point cell counts had declined to less than 20 cfu ml⁻¹ from an initial density after inoculation of around 10⁸ cfu ml⁻¹, and no further chemical changes were observed. Vanadium reduction began within 20 min of inoculation as shown by the rapid development of blue colour in the medium and V in solution stabilized at around 0.1 mM by 30 h (Fig. 2). The concentration of U in solution quickly decreased and remained low; this decrease corresponded to the formation of a dark, fine grained precipitate visible in the culture bottles. Uranium in solution also decreased rapidly in the bacteria-free control, which corresponded to the appearance of white precipitates, likely uranium phosphate minerals based on SEM imaging and EDS analysis (Appendix C).

3.3. Changes in chemistry and mineralogy during incubation of carnotite group minerals

Oxygen K-edge NEXAFS is an excellent probe for the covalency of actinide-oxide bonds (Wu et al., 1999; Minasian et al., 2013; Wen et al., 2014). Initial STXM investigations of uranium oxides have shown that the 4d_{5/2} edge is the most useful absorption edge for STXM in the soft X-ray region above ~100 eV. In the case of uranium, this edge has a

reproducible charge state shift of ~1.3 eV from uranium (IV) dioxide to uranium (VI) trioxide (Kalkowski et al., 1987; Nilsson et al., 2005). There have been several studies of metallic uranium compounds at the 4d edges (Kalkowski et al., 1987; Van der Laan et al., 2004). A useful comparison is to the actinide metallic counterparts of the dioxides at the 4d_{5/2} edge from these studies. The differences in band structures for actinide metal versus actinide dioxide can lead to 4d_{5/2} edge peaks with different widths. This has been observed in the NEXAFS of transition metals and transition metal oxides (de Groot, 1991). For vanadium, the 2p (L_{2,3}) absorption spectra are useful to detect oxidation states of V(V), V(IV) and V(III) (Cressey et al., 1993; Abbate, 1994; Maganas et al., 2014). Using STXM, we identified V(V) and V(IV) during the incubation with the U-sandstone. In support of our initial visual observations, V(IV) was detected 1 d after inoculation and was the dominant oxidation state detected in association with the bacteria, although V(III) was also detected during the 10 month period. Some V persisted as V(V) throughout, supporting that chemical transformation of the U-bearing minerals was incomplete. In contrast, U was detected only as U(VI) (Fig. 4). Differences in the spatial distribution of U and V developed over time, as observed on regions of the solid material (Fig. 5), and which is consistent with the detection of V(IV). Fine precipitates formed that appeared to coat larger mineral grains and bacteria (Fig. 3d).

The concentration of Fe was relatively low in the fine fractions (Table 1). The iron valency appeared to be stable as Fe(III) throughout the incubation; STXM analysis showed areas of high Fe concentration as particulates. We also examined the sand fraction and fine fractions that formed distinct layers during the incubation using XRD. The sand fraction contained quartz, with traces of cristobalite and feldspar (sanidine) (Fig. 1). In the fine fraction, refinement of the data indicated a mixture

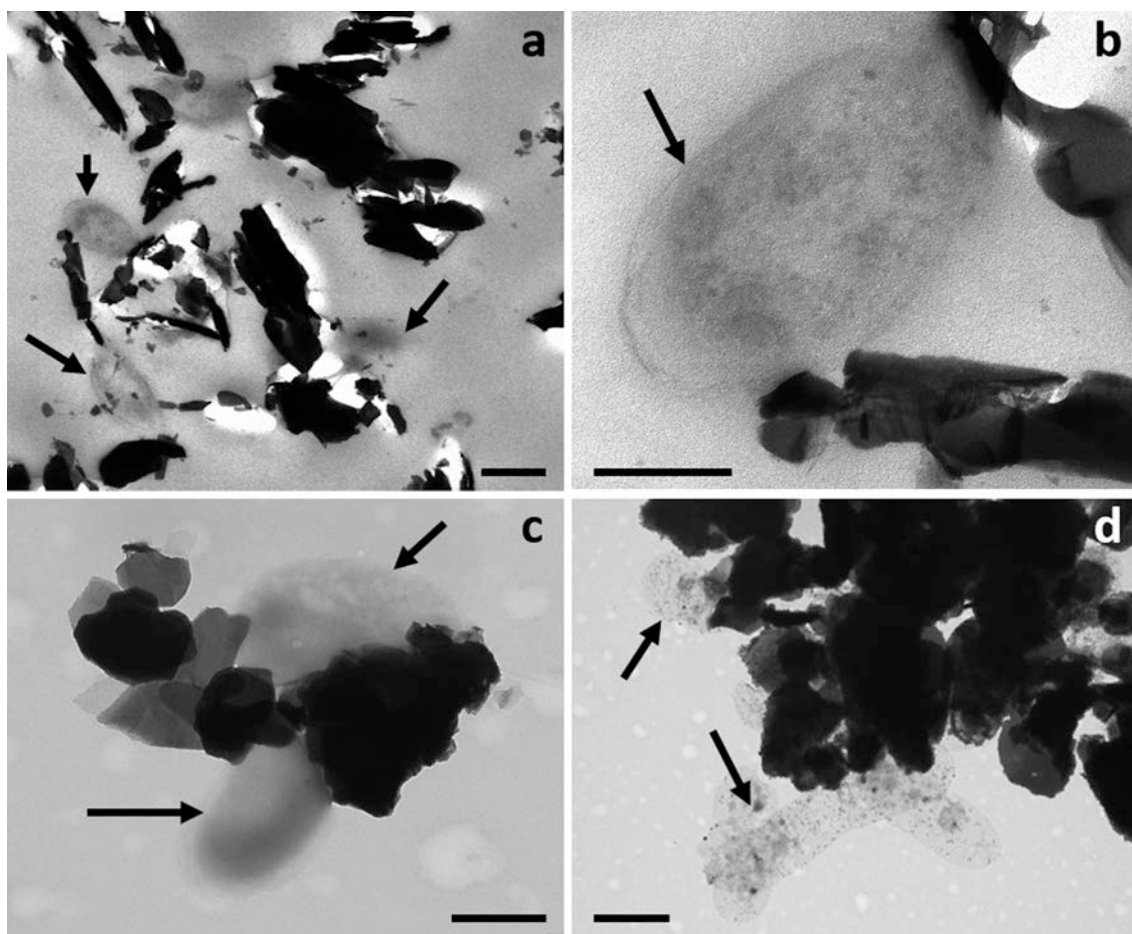


Fig. 3. Transmission electron micrographs showing the association of CN32 with U-ore minerals. a) and b) thin sections of cultures after 3 days; c) whole mount preparation of culture after 3 days; d) whole mount preparation of 4-month culture. Arrows indicate bacteria; scale bars are 500 μm (a, c, d) and 250 μm (b).

of K-carnotite, which belongs to the monoclinic space group, and metatyuyamunite. This fraction was enriched in K and depleted in Ca compared to the initial yellow fine fraction (Table 1), consistent with the appearance of carnotite. Fritzscheite was not detected even though Mn and Ba concentrations in the fine fraction were relatively unchanged after incubation (Table 1). Observations using SEM showed mineral particles that had a platy structure similar to that seen for the initial U-bearing minerals, but the plates were thinner and formed rosettes (Appendix C). SEM-EDS indicated elevated concentrations of P in association with U for these structures, suggesting autunite [$\text{Ca}(\text{UO}_2)_2(\text{PO}_4)_2 \cdot 10\text{--}12(\text{H}_2\text{O})$], which can also accommodate Na and K. Autunite could not be confirmed by bulk XRD likely because of very low abundance, but it is supported by STXM results (Fig. 4). Distinct particles of vanadium oxide (VO_2) were observed in association with the bacteria by STXM (discussed below) but were also not detected by bulk XRD. There was no chemical, mineralogical, or visual evidence for a distinct UO_2 component.

3.4. Associations between bacteria, U and V

3.4.1. Carnotite group mineral ore

STXM images show the bacteria were closely associated with nm and micron-sized particles of the CGM. (Fig. 5). Wet samples imaged using STXM after one week revealed bacteria embedded in an extensive exopolymer matrix that contained protein, lipids, and polysaccharides, consistent with biofilm formation and growth, with distinct mineral particles distributed heterogeneously within the biofilm matrix (Appendix B). Over time, the bacteria appeared to associate preferentially as

individuals or as clusters of few cells with the CGM. Sparse, fine (2–3 nm) precipitates accumulated on the bacteria (Fig. 3d). We did not observe U or V precipitates in the periplasm or cytoplasm of CN32 during the incubation of CGM, as assessed by TEM observations on thin sections. This supports that metal reduction took place outside the cell, consistent with the location of metal reducing enzymes at the outer leaflet of the outer membrane (Myers and Myers, 1992).

Elemental maps of the solid phase after 8 months show the close correspondence between V, U, Ba, Ca and K (Appendix A).

3.4.2. Soluble U and V

After inoculation with CN32, the medium became light blue within two hours, indicating reduction of V(V) to V(IV). Fine precipitates accumulated in the periplasm of the bacteria and external to the cell during the incubation, as observed by TEM on thin sections and reported by others for dissimilatory U(VI) reduction (e.g., Lloyd et al., 2002). Bacteria formed flocs containing an abundant matrix of exopolymeric substances (EPS) during reducing conditions. The EPS contained proteins, lipids and carbohydrates, and is chemically similar to the biofilms observed for the CGM treatment, as indicated by STXM (data not shown). Uranium and vanadium appeared to concentrate in the extracellular matrix (Fig. 6). After 24 h, we detected U(IV) and V(III) within the matrix of bacteria, exopolymer and mineral solids. Uranium (VI), V(V) and V(IV) were not detected after 24 h (Fig. 6).

3.5. Growth inhibition and biofilm assays

Because of the longevity of CN32 in the U-ore treatments compared

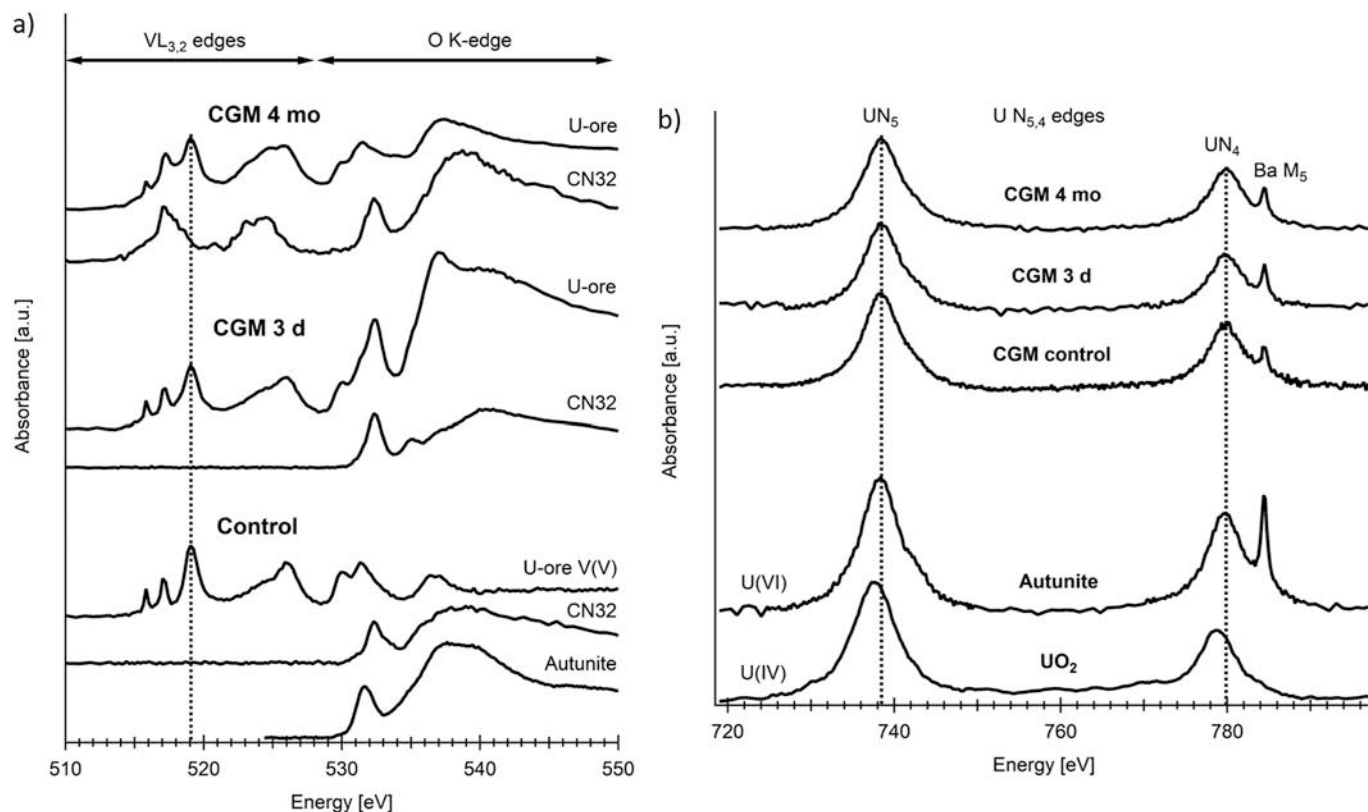


Fig. 4. STXM-derived Vanadium 2p core absorption spectra (left) and Uranium 4d core spectra (right) showing changes during incubation with *Shewanella putrefaciens* CN32. V L_{2,3} absorption maxima shift to lower energy values with reduction from V⁵⁺ to V⁴⁺ in the range from 514 to 520 eV (indicative V(V) dashed line at 519.1 eV) and 524–526 eV. U d absorption maxima shift around 1.3 eV to lower energy with reduction from U(VI) to U(IV), from 780 eV to 778.7 eV (N₄ edge), and from 738 eV to around 737 (N₅ edge) (dashed lines, right), which was not observed for the U-ore treatments.

to those with soluble U and V, we tested growth inhibition over a range of U(VI) and V(IV) concentrations. Vanadyl [V(IV)] was included rather than V(V) because it was the form of V present in association with bacteria during the incubation with the U-ore, whereas U(VI) was the only observed oxidation state of U in the same treatment. Vanadyl is stable in solution against oxidation for at least 24 h (French et al., 2013a). To maintain these oxidation states of U and V, the assays were conducted under aerobic conditions, with the understanding that CN32 adjusts cell wall biochemistry in response to oxygen presence (French et al., 2013a). The results should, therefore, be interpreted qualitatively and to compare relative responses to different metal concentrations. *Escherichia coli*, well studied as a model Gram-negative organism, was included as a reference strain (K 12). Calcium was included as a cation which, at the tested concentrations, would not have negative impact on cell growth. Calcium ions have important roles in maintaining cell wall health and affect fundamental processes such as bacterial adhesion (Ilangovan et al., 2001; Naik et al., 2006). Calcium and V(IV) did not inhibit growth at any of the tested concentrations, for both bacterial species. *S. putrefaciens* was 100-fold more sensitive to the presence of U(VI) than was *E. coli*, with growth suppressed at concentrations of 0.01 and 1 mM respectively. *E. coli* strains in general have shown tolerance to a wide range of metals (Nies, 2007).

The influence of these soluble metals on the formation and growth of biofilms was also investigated. As noted earlier, cells surrounded by EPS were intimately associated with the carnotite group minerals or occurred as flocs following incubation with U and V species; both are consistent with descriptions of bacterial growth as a biofilm. To assess biofilm development in the presence of dissolved V and U, biofilms were assessed as staining of biomass attached to glass test tubes, shown by the band thickness and density (Fig. 7). Dense biofilms were formed at all concentrations tested of Ca and V for CN32, but only at the lowest

concentration of U, 0.001 mM. At this concentration, the amount of biofilm was increased by 30% relative to the control. The stimulation of biofilm growth by sub-inhibitory concentrations of U is reminiscent of bacterial responses to environmental stresses such as sub-inhibitory concentrations of antibiotics (Andersson and Hughes, 2014). In contrast, *E. coli* did not show increased biofilm formation in response to sub-inhibitory U(VI) and formed less abundant biofilms overall (Fig. 7). The outer membrane of *S. putrefaciens* is known to be perturbed by uranium (French et al., 2013a), with the possible induction of stress responses (reviewed in Kolhe et al., 2018). Vanadium stimulated biofilm growth of *S. putrefaciens* at 1 mM only, with values increasing by 60% relative to the control; lower concentrations of V yielded values similar to the control. Calcium had little impact on biofilm growth.

4. Discussion

4.1. U and V chemical transformations

The reduction of naturally occurring, solid phase U(VI) has been demonstrated to date only for U(VI) precipitates located between larger lithic fragments (Liu et al., 2009). We did not observe a net chemical reduction of U(VI) in CGM, in agreement with other studies that did not observe U(VI) reduction when different U-containing minerals were incubated with metal reducing bacteria (Ilton et al., 2006; Smeaton et al., 2008). This outcome is likely due to steric and bonding considerations (Stohl and Smith, 1981), similar to limits on Fe reduction observed under nutrient limited conditions (Glasauer et al., 2003).

In contrast to U(VI), a portion of the V(V) in the CGM was readily reduced. Based on half-cell reduction potentials, V(V) in pure solution under standard conditions can be expected to reduce to V(IV) more readily than Fe(III) → Fe(II) or U(VI) → U(IV) (Lee, 1992). The chemical

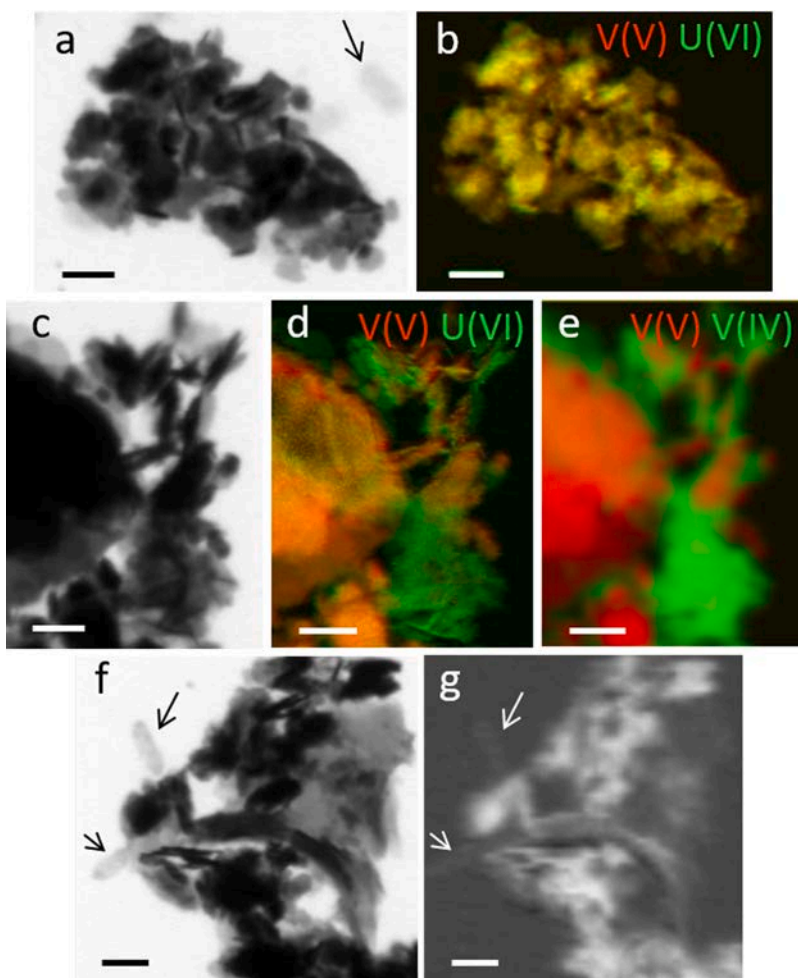


Fig. 5. Changes over time in the spatial distribution of uranium and vanadium during incubation of *Shewanella putrefaciens* with uranium ore, as shown by scanning transmission X-ray microscopy. After 3 days: a) STXM image recorded at 518.5 eV showing bacteria and particles b) chemical map indicating colocalization of V(V) and U(VI). After 4 months: c) STXM image recorded at 518.5 eV and d) corresponding chemical map showing distinct V(V) and U(VI) phases and e) chemical map evidencing V(V) and V(IV), derived from stack fitting using larger pixel size. U(VI) is mainly colocalized with V(IV) and not with V(V). f) STXM image recorded at 518.5 eV at 4 months and g) corresponding V map (derived from a “stack”) showing that bacteria contain vanadium. Uranium was not detected on the cells. See corresponding spectra in Fig. 4. Arrows point to bacteria. Scale bars are 1 μm .

form of the metal and the chemical conditions will clearly impact reducibility (Cumberland et al., 2016). The reduction potentials for U or V contained in CGM is unknown. In addition, the ore that we used contained at least two distinct uranyl vanadate minerals, metatyuyamunite and fritzscheite, and it was not possible to observe their behavior separately during the incubation. It is likely that the minerals were not chemically pure due to element substitutions and traces of other associated elements.

The presence of V(III) species observed during reduction of the CGM stands in contrast to the lack of U(VI) reduction; V(III) indicates strongly reducing conditions (Wehrli and Stumm, 1989). In a related study, V(III) was not detected in the bulk solution when CGM was incubated with CN32 under identical culture conditions, although V(III) was observed during the dissimilatory reduction of V(V) added as a sodium vanadate salt (Li et al., 2007). Although the STXM results present a consistent picture of U and V chemistry during the incubation, it is feasible that local areas may have contained U(IV) that was below detection limits or was not examined. In contrast, U(IV) was detected consistently in the treatments with soluble V(V) and U(VI) using STXM (Fig. 6). V(III) was also detected (Appendix D); however, we cannot rule out beam-induced damage on this dataset. Overall, these data suggest more highly reduced conditions.

The geochemistry of vanadium is particularly complex. Vanadium exists in multiple states of oxidation, hydrolysis, and polymerization (Macara, 1980; Huang et al., 2015). Pentavalent species are especially prone to polymerize; at concentrations as low as 1 mM and neutral pH, HVO_4^{2-} aggregates into trimers and tetramers. Vanadate species, similar in chemical behavior to phosphate, readily form polynuclear complexes

with phosphate as well as surface complexes with hydrous oxides (Wehrli and Stumm, 1989). The redox transition for V(V)-V(IV) occurs at E_H values comparable to those for Mn(II)-Mn(IV), around 0.1–0.5 V, which is characteristic for sediment-water interfaces (Wehrli and Stumm, 1989). Vanadyl species in many natural waters are predicted to hydrolyze, sorb strongly to mineral surfaces, and are considered relatively insoluble (Wehrli and Stumm, 1989; Huang et al., 2015). The gradual disappearance of total V from solution correlates with the accumulation of V(IV) and V(III) precipitates observed on the bacteria, likely as $\text{VO}(\text{OH})_2$ and V_2O_3 . Vanadium(III) species are highly insoluble except in acidic conditions (below pH 2) and in the absence of O_2 (Macara, 1980).

4.2. Mineral transformations

The minerals in the U-sandstone were transformed by two main processes: 1) bacterial dissimilatory reduction of V(V), and 2) exchange of cations contained in the interlayer of the carnotite group minerals. The incubation studies with CGM illustrate how biotic and abiotic processes can simultaneously affect mineral transformation. Given that U(VI) and V(V) only coexist in mineral form when both are oxidized (Langmuir, 1978), the bacterial reduction of V(V) would necessarily release both metals. The separation of V and U consequent to V reduction is supported by the appearance of V oxide particles on the bacteria and the appearance of distinct solids containing U and P. Soluble U was not detected during the transformation of CGM. The high affinity of U for adsorption to organic matter and minerals would scavenge dissolved U, which could help foster the precipitation of U phases. Precipitates of

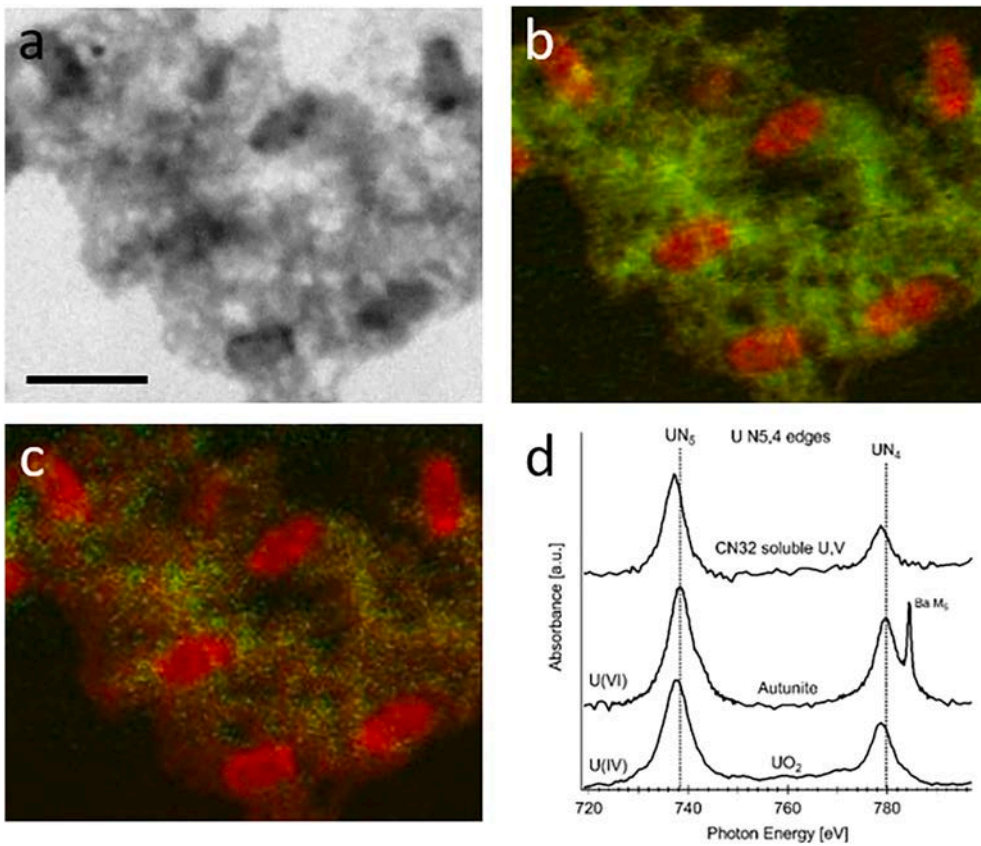


Fig. 6. STXM-derived elemental distribution and chemical speciation of uranium in CN32 samples during the reduction of soluble V, U after three days. a) STXM image recorded at 307 eV. Scale bar is 2 μm . Corresponding element maps showing b) carbon in red, vanadium in green, c) carbon in red, uranium in green, vanadium in blue. d) U $N_{4,5}$ edges NEXAFS spectra showing that U is present as U(IV). (For interpretation of the references to colour in this figure legend, the reader is referred to the web version of this article.)

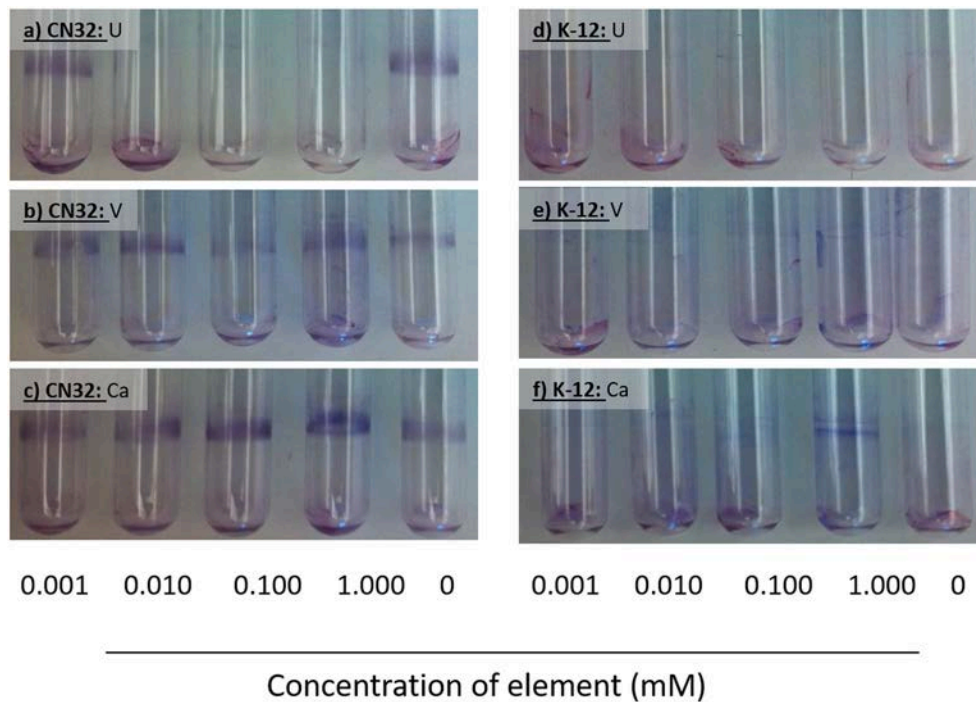


Fig. 7. Biofilm formation of *Shewanella putrefaciens* CN32 and *E. coli* K-12 in response to U(VI) (a,d), V(IV) (b, e) and Ca (c, f). The amount of retained crystal violet stain indicates the amount of biomass adhered to the sides of the glass tubes after 20 h incubation in the presence/absence of added elements. (For interpretation of the references to colour in this figure legend, the reader is referred to the web version of this article.)

fine-grained V- and U-containing phases that formed during the incubation could only be indirectly assessed for mineral properties, i.e., using SEM, TEM and STXM. These nanometer-scale particles can be directly linked to the microbial transformation of V(V) contained in the U-sandstone minerals. STXM elemental maps revealed regions where U appeared to be distinct from V, suggesting separation.

Mineral formation was likely fostered by the controlled conditions of our experiments, e.g., the concentration of K in the culture medium likely favored CGM over fritzscheite. The limits to cation substitution for the interlayer of the UO_2VO_4 sheets have not been established. The elements that comprise the distinct variants include K, Pb, Ba, Mn, Cs, Ca, Cu, Na, and Al (no Fe variant is known) (Finch and Murakami, 1999), although it is feasible that additional substituted cations could occur in low concentrations. In addition, structural water in the interlayer can vary. For example, hydration-dehydration for tyuyamunite is reversible for water contents ranging from 3 to 8.5 H_2O , with meta-tyuyamunite at the lower end of that range. (Stern et al., 1956). The optical properties and XRD patterns of the CGM variants are distinct, analogous to the behavior of swelling clays such as montmorillonite that respond similarly to hydration or exposure to cations having different radii. Although these transformations were a consequence of experimental conditions, they illustrate the flexible response of the minerals to changes in their chemical surroundings, on short time scales, which can have implications for mineral solubility. For example, carnotite is less soluble than tyuyamunite under some conditions (Hostetler and Garrels, 1962; Weeks, 1961). Carnotite group members typically occur together in complex assemblages which cannot be physically separated and respond readily to environmental conditions (Stern et al., 1956; Finch and Murakami, 1999).

In addition, the microscopy studies – both SEM and STXM – support that autunite formed during the incubation, suggesting that U(VI) that was released from the U-ore minerals was immobilized by precipitation with phosphate.

4.3. Reactions at bacteria-mineral and bacteria-metal interfaces

The lack of periplasmic precipitates during the dissimilatory reduction of V in CGM supports that reduction took place at the interface between the cell wall and the extracellular environment. For Gram negative bacteria, the outer and plasma membranes sandwich the periplasm, a gel-like region that contains proteins involved in shuttling chemicals and electrons between the outer membrane and the cytoplasm. Shuttling factors include soluble cytochrome proteins that can reduce soluble, oxic forms of metals during anaerobic respiration. If the reduced form of the metal is insoluble, nano-sized precipitates form in the periplasm, as documented for U and Tc (e.g., Lloyd et al., 2002) and observed during the reduction of soluble V and U in our treatments.

It is unknown how bacteria that respire metals maintain critical chemical gradients and membrane fluidity, and continue to uptake nutrients, when bulk conditions favor the sorption of metals and minerals to the cell envelope (French et al., 2013b). Bacteria are highly interactive with dissolved metal ions due to a high surface-to-volume ratio and a high density of metal-reactive functional groups in the cell wall (Beveridge, 1989). They develop extracellular gradients by actively and passively taking up and expelling metals and other chemical species. As a result, the interface between the cell wall and the immediate extracellular environment differs in metal composition and concentration from the bulk suspending fluid. Metal speciation is also a factor; for example, the rate of Fe^{3+} reduction has been shown to depend on the form of the metal that is present: soluble, complexed, sorbed or mineral (Urrutia et al., 1998; Zachara et al., 1998; Haas and DiChristina, 2002; Glasauer et al., 2003). Cell respiration may contribute to keeping metals in solution near bacteria through H^+ efflux. For example, more acidic pH values were observed proximal to bacteria in a biofilm, relative to the bulk exopolymer, which was suggested to increase metal solubility (Hunter and Beveridge, 2005). Bacteria have biochemical responses to

environmental change that may help them resist the impacts of soluble metals on the cell wall. In earlier research, we observed that *S. putrefaciens* CN32 altered lipid chemistry in response to uranium and vanadium, as well as in response to oxygen, which may impact the accumulation of these elements (French et al., 2013a). In the case of the treatments with soluble U and V, the accumulation of these elements in the exopolymer matrix and their exclusion from the bacteria suggest distinct microenvironments, although this remains speculative.

Our results support that biofilms and flocs of CN32 immobilize U, as shown by others for U in the presence of microbes in controlled studies (reviewed in Cao et al., 2011; Cologgi et al., 2014; Stylo et al., 2013). Immobilization has been demonstrated in a field study of natural biofilms (Amano et al., 2017) and in natural organic matter associated with surface and subsurface sediments (Bone et al., 2017; Bone et al., 2020). In particular, Cao et al. (2011) showed that adsorption of U(VI) is competitive between EPS and cells of *Shewanella* HRCR-1, with a higher proportion of U(VI) associated with EPS when U(VI) concentrations were lower. This study (Cao et al., 2011) also showed that the presence of EPS did not affect the reduction efficiency of U(VI) to U(IV), with around 60% of U(VI) reduced at a concentration of 1 mM, identical to the concentration we used to investigate reduction of soluble U(VI) and V(V). Microorganisms respond to environmental stresses such as nutrient limitation as well as to antimicrobial stress by producing EPS (e.g., Myszka and Czaczky, 2009; Andersson and Hughes, 2014). The response of CN32, in terms of growth and proliferation of exopolymeric substances (EPS), may enhance survival by keeping U species from interacting with membrane lipids, which decreases membrane fluidity (French et al., 2013a). The role of EPS in binding potentially toxic elements is not well understood, largely due to differences in methodology (reviewed in Butzen and Fein, 2019). We speculate that the binding of U to high affinity sites in EPS, as observed for Cd (Butzen and Fein, 2019), would favor bacterial survival. We cannot, however, infer that the response of CN32 to the lowest concentration of U in our study of biofilm formation is unequivocally a defense mechanism. It is nevertheless remarkable that CN32 responds in a way that appears to keep U away from the cell wall. Our observation that this occurs particularly at sub-inhibitory concentrations of U suggests that EPS formation and reduced toxicity are linked. A link between EPS and reduced toxicity to bacteria may also help to explain why the response to V occurred only at much higher concentrations, given the relatively low toxicity of V.

A change from oxidizing to reducing conditions, such as at redox transition zones, may mobilize V in the short term from carnotite-type minerals. Uranium (VI) species that are released consequently will sorb to minerals and precipitate at low ion activity; however, it should be kept in mind that the affinity of U species for organic matter is particularly high (reviewed in Cumberland et al., 2016). In one study, this affinity had a greater impact on U mobility than did complexation by carbonate species, despite thermodynamic predictions (Yang et al., 2012). In our studies, U did not become soluble when the CGM were transformed under reducing conditions, indicated by the lack of U in solution or associated with cells in this treatment. If V and U remain in pore water and adsorbed to solids, a return to oxidizing conditions could induce the precipitation of uranyl vanadate minerals (Tokunaga et al., 2009; Tokunaga et al., 2012). The strong interaction of U(VI) with organic matter is speculated to have immobilized and concentrated U in the Colorado Plateau environment (Cumberland et al., 2016; Spirakis, 1996; Hansley and Spirakis, 1992) with eventual precipitation.

4.4. Implications for ore formation

The formation of carnotite-type deposits is controversial. In the Colorado Plateau, it has been hypothesized that cycles of reducing and oxidizing conditions have created the present roll front and tabular structures that characterize the deposits (Weeks, 1961; Hostetler and Garrels, 1962). V(III) and U(IV) existing separately in primary reduced minerals would have mobilized upon exposure to moderately oxidizing

conditions in weathering environments. Transport as U(VI) and V(IV) species under slightly reducing (-0.1 V), alkaline conditions is one proposed scenario (Evans and Garrels, 1958; Weeks, 1961). These redox conditions are similar to those created during the anoxic incubation of CN32 with the CGM. It is likely that U and V were transformed during cycles of oxidizing and reducing conditions; reducing conditions would have prevailed, for example, in the organic-rich Triassic deposits which may have been infiltrated by U-bearing fluids during the Jurassic period (Hansley and Spirakis, 1992; Spirakis, 1996). Subsequent oxidizing conditions would have led to the mobilization and ultimate coprecipitation of V and U as carnotite-type minerals. Bacterial activity may continue to exert an important control on the mobility of both U and V in the subsurface environment of the Colorado Plateau today.

5. Conclusions

Our results support previous studies in demonstrating the resistance of mineral U(VI) to bacterial reduction. In contrast to those studies, however, the carnotite group minerals include an alternate oxidized element, V(V), that readily served as an electron acceptor in our experiments. Reduction of mineral-bound V(V) did not liberate U into solution; instead, there was evidence that autunite was formed. The initial carnotite group mineral fritzscheite was transformed to K-carnotite through the replacement of interlayer cations, indicating that mineral changes were induced through biotic and abiotic pathways. In contrast to our investigations with mineral U and V, soluble V(V) and U(VI) were readily reduced in the presence of metal-respiring bacteria. The abundant exopolymer matrix which surrounded the bacteria during respiration of the soluble electron acceptors appeared to accumulate these elements in preference to bacterial surfaces. This suggests that the

biofilm matrix helped to reduce the exposure of bacteria in particular to U, which is highly toxic. Understanding the role of biofilms in ameliorating toxicity is important given that exopolymeric substances are produced by bacteria in response to environmental conditions.

Natural environments contain many possible electron acceptors for bacteria that can adapt readily to challenging conditions. Understanding the relative availability of electron acceptors from the microbial perspective is key to interpreting element solubility and mineral transformation reactions in the present – and perhaps in the past.

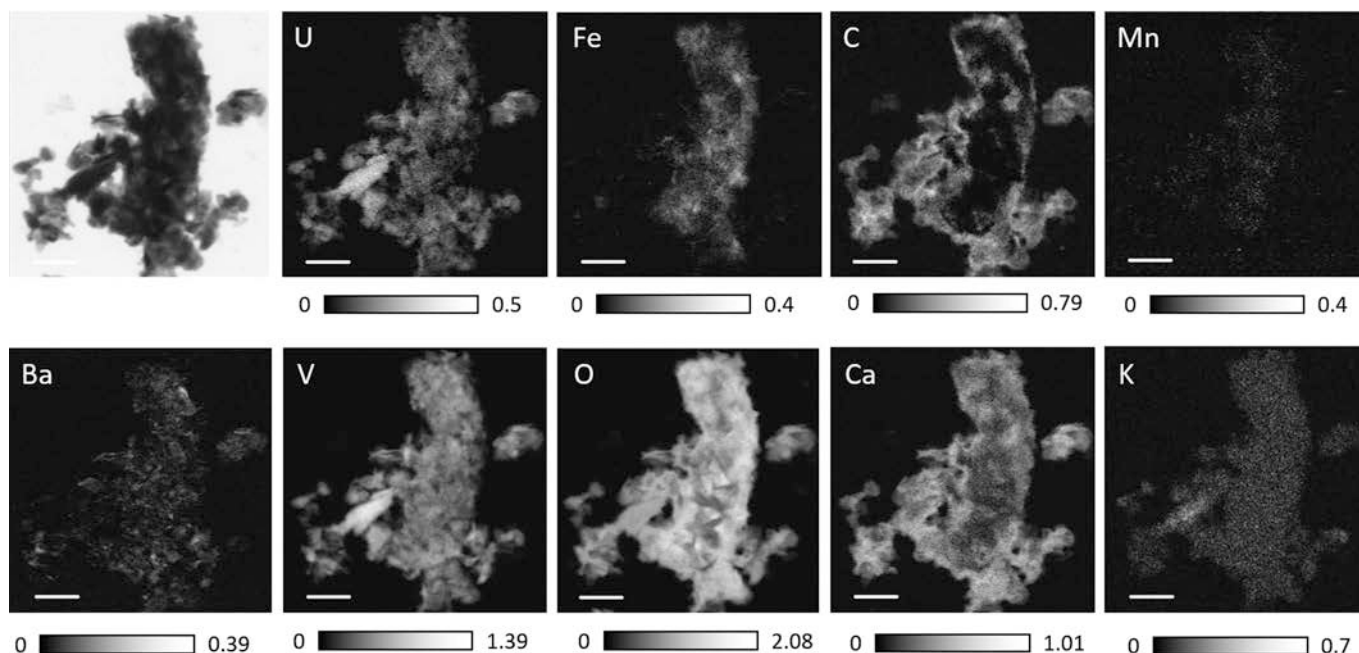
Aknowledgements

The authors are grateful to Brian S. Fairchild of LBNL EH&S for his help with the STXM experiments. We thank Farhana Islam and Christine Cousins for assistance with the culture experiments at the University of Guelph and Dr. Susan Koval (University of Western Ontario: London, ON, Canada) for provision of *E. coli* K-12 (AB264 lineage). This research was supported by the Natural Science and Engineering Research Council (NSERC) through a Discovery grant to S. Glasauer. Parts of this research, the ALS, and the ALS-MES Beamline 11.0.2 were supported by the Director, Office of Science, Office of Basic Energy Sciences, Division of Chemical Sciences, Geosciences, and Biosciences and Materials Sciences Division of the U.S. Department of Energy at the Lawrence Berkeley National Laboratory under Contract No. DE-AC02-05CH11231 (SF, DKS, TT).

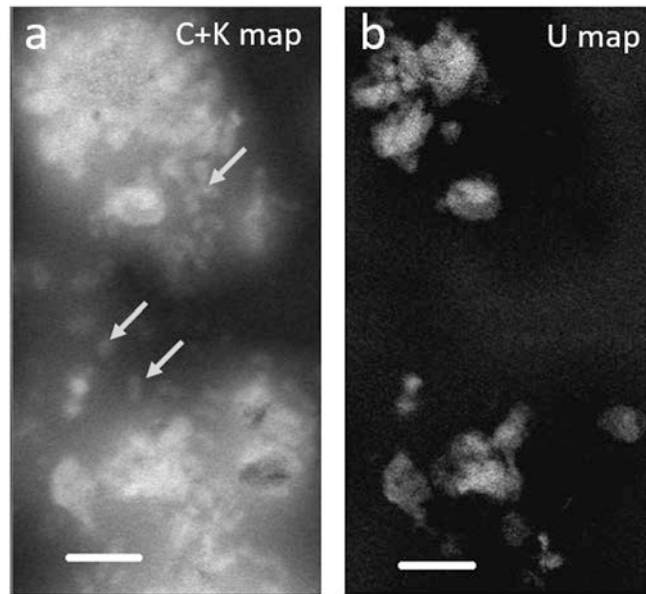
Declaration of Competing Interest

None of the authors has a competing interest for this research.

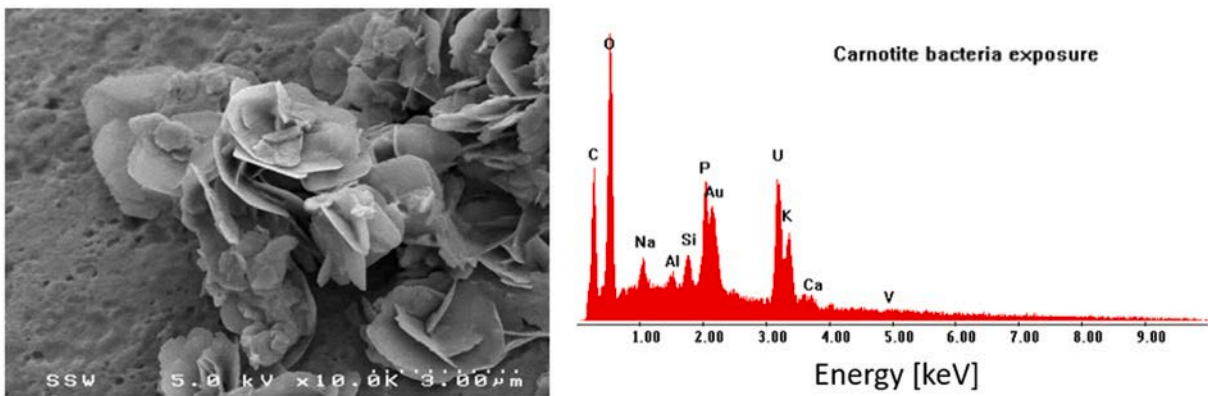
Appendix A. STXM image recorded at 738 eV (U N5 -edge) and STXM-derived elemental maps of carnotite after incubation with CN32 for 8 months. Scale bars are 2 μ m



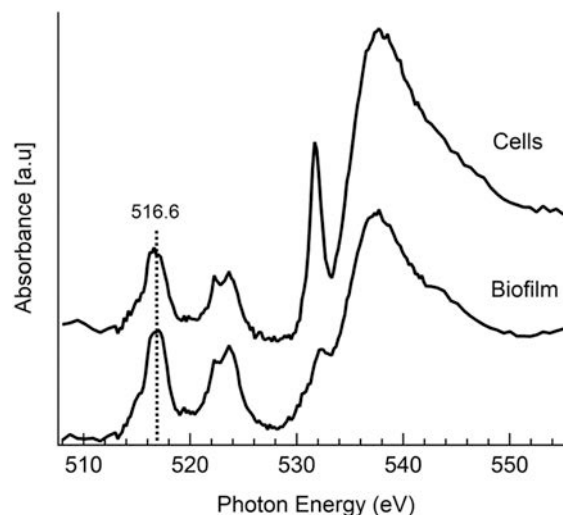
Appendix B. STXM-derived elemental maps (at C K and U N_{4,5} edges) of hydrated samples after 1 week incubation with U ore, showing abundant C matrix with potassium associated with embedded bacterial cells (a). The bacteria are not strongly associated with U (b). Scale bars are 500 μ m. Arrows point to cells



Appendix C. Minerals containing U and P formed during the incubation of CN32 with uranium sandstone ore



Appendix D. STXM-derived VL_{2,3} and O–K edges NEXAFS spectra of CN32 samples during the reduction of soluble V, U after three days suggesting the presence of V(III)



References

- Abbate, M., 1994. The O 1s and V 2p X-ray absorption spectra of vanadium oxides. *Braz. J. Phys.* 24, 785–795.
- Amano, Y., Iwatsuki, T., Naganuma, T., 2017. Characteristics of naturally grown biofilms in deep groundwaters and their heavy metal sorption property in a deep subsurface environment. *Geomicrobiol J.* 34, 769–783.
- Anderson, R.T., Vrionis, H.A., Ortiz-Bernad, I., Resch, C.T., Long, P.E., Dayvault, R., Karp, K., Marutzky, S., Metzler, D.R., Peacock, A., White, D.C., Lowe, M., Lovely, D. R., 2003. Stimulating the in situ activity of *Geobacter* species to remove uranium from the groundwater of a uranium-contaminated aquifer. *Appl. Environ. Microbiol.* 69, 5884–5891.
- Andersson, D.I., Hughes, D., 2014. Microbiological effects of sublethal levels of antibiotics. *Nat. Rev. Microbiol.* 12, 465–478.
- Bargar, J.R., Williams, K.H., Campbell, K.M., Long, P.E., Stubbs, J.E., Suvorova, E.I., Lezama-Pacheco, J.S., Alessi, D.S., Stylo, M., Webb, S.M., Davis, J.A., Giammar, D.E., Blue, L.Y., Bernier-Latmani, R., 2013. Uranium redox transition pathways in acetate-amended sediments. *Proc. Natl. Acad. Sci.* 110, 4506–4511.
- Beveridge, T.J., 1989. Metal ions and bacteria. In: Beveridge, T.J., Doyle, R.J. (Eds.), *Metal Ions and Bacteria*. John Wiley and Sons, New York.
- Bluhm, H., Andersson, K., Araki, T., Benzerara, K., Brown, G.E., Dynes, J.J., Ghosal, S., Gilles, M.K., Hansen, H.-Ch., Hemminger, J.C., Hitchcock, A.P., Kettler, G., Kilcoyne, A.L.D., Kneeder, E., Lawrence, J.R., Leppard, G.G., Majzlam, J., Mun, B.S., Myneni, S.C.B., Nilsson, A., Ogasawara, H., Ogletree, D.F., Pecher, K., Salmeron, M., Shuh, D.K., Tonner, B., Tylliszczak, T., Warwick, T., Yoon, T.H., 2006. Soft X-ray microscopy and spectroscopy at the molecular environmental science beamline at the Advanced Light Source. *J. Electron Spectrosc. Relat. Phenom.* 150, 86–104.
- Bone, S.E., Cahill, M.R., Jones, M.E., Fendorf, S., Davis, K.H.W., Bargar, J.R., 2017. Oxidative uranium release from anoxic sediments under diffusion-limited conditions. *Environ. Sci. Technol.* 51, 11039–11047.
- Bone, S.E., Cliff, J., Weaver, K., Takacs, C.J., Roycroft, S., Fendorf, S., Bargar, J.R., 2020. Complexation by organic matter controls uranium mobility in anoxic sediments. *Environ. Sci. Technol.* 54, 1493–1502.
- Butzen, M.L., Fein, J.B., 2019. Influence of extracellular polymeric substances on the adsorption of cadmium onto three bacterial species. *Geomicrobiol J.* 36, 412–422.
- Cao, B., Ahmed, B., Kennedy, D.W., Wang, Z., Shi, L., Marshall, M.J., Fredrickson, J.K., Isern, N.G., Majors, P.D., Beyenal, H., 2011. Contribution of extracellular polymeric substances from *Shewanella* sp. HRCR-1 biofilms to U(VI) immobilization. *Environ. Sci. Technol.* 45, 5483–5490.
- Carpentier, W., Sandra, K., De Smet, I., Brigé, A., De Smet, L., Van Beeumen, J., 2003. Microbial reduction and precipitation of vanadium by *Shewanella oneidensis*. *Appl. Environ. Microbiol.* 69, 3636–3639.
- Carpentier, W., Smet, De, Beumen, Van, Brigé, A., 2005. Respiration and growth of *Shewanella oneidensis* MR-1 using vanadate as the sole electron acceptor. *J. Bacteriol.* 187, 3293–3301.
- Cologgi, D.L., Speers, A.M., Bullard, B.A., Kelly, S.D., Reguera, G., 2014. Enhanced uranium immobilization and reduction by *Geobacter sulfurreducens* biofilms. *Appl. Environ. Microbiol.* 80, 6638–6646.
- Cressey, G., Henderson, C.M.B., van der Laan, G., 1993. Use of L-edge X-ray absorption spectroscopy to characterize multiple valence states of 3d transition metals; a new probe for mineralogical and geochemical research. *Phys. Chem. Miner.* 20, 111–119.
- Cumberland, S.A., Douglas, G., Grice, K., Moreau, J.W., 2016. Uranium mobility in organic matter-rich sediments: a review of geological and geochemical processes. *Earth Sci. Rev.* 159, 160–185.
- de Groot, F.M.F., 1991. Ph.D. Thesis, X-Ray Absorption of Transition Metal Oxides. University of Nijmegen, Nijmegen, Netherlands.
- DiChristina, T.J., Fredrickson, J.K., Zachara, J., 2005. Enzymology of electron transport: Energy generation with geochemical consequences. In: Banfield, J.F., Cervini-Silva, J., Nealon, K.M. (Eds.), *Reviews in Mineralogy and Geochemistry*, vol. 59. Mineralogical Society of America, Washington, D.C., pp. 27–52.
- Eckstrom, A., Fooks, C.J., Hambley, T., Loeh, H.J., Miller, S.A., Taylor, J.C., 1983. Determination of the crystal structure of a porphyrin isolated from oil shale. *Nature* 306, 173–174.
- Evans, H.T., Garrels, R., 1958. Thermodynamic equilibria of vanadium in aqueous systems as applied to the interpretation of the Colorado Plateau ore deposits. *Geochim. Cosmochim. Acta* 15, 131–149.
- Evans, H.T., White, J.S., 1987. The colorful vanadium minerals: a brief review and a new classification. *Mineral. Rec.* 18, 333–340.
- Finch, R., Murakami, T., 1999. Systematics and paragenesis of uranium minerals. In: Burns, P.C., Finch, R. (Eds.), *Uranium: Mineralogy, Geochemistry and the Environment; Reviews in Mineralogy*, vol. 38, pp. 91–180.
- Fredrickson, J.K., Zachara, J.M., Kennedy, D.W., Dong, H., Onstott, T.C., Hinman, N.W., Li, S., 1998. Biogenic iron mineralization accompanying the dissimilatory reduction of hydrous ferric oxide by a groundwater bacterium. *Geochim. Cosmochim. Acta* 62, 3239–3257.
- Fredrickson, J.K., Zachara, J.M., Kennedy, D.W., Duff, M.C., Gorby, Y.A., Li, S.-M., Krupka, K.M., 2000. Reduction of U(VI) in goethite suspensions by a dissimilatory metal-reducing bacterium. *Geochim. Cosmochim. Acta* 64, 3085–3098.
- French, S., Fakra, S., Trevors, Glasauer, S., 2013a. Changes in *Shewanella putrefaciens* CN32 membrane lipid chemistry and fluidity in the presence of soluble Mn(II), V (IV), and U(VI). *Geomicrobiol J.* 30, 245–254.
- French, S., Puddephatt, D., Habash, M., Glasauer, S., 2013b. The dynamic nature of bacterial surfaces: Implications for metal-membrane interaction. *Crit. Rev. Microbiol.* 39, 196–217.
- Glasauer, S., Langley, S., Beveridge, T.J., 2001. Sorption of Fe(hydr)oxides to the surface of *Shewanella putrefaciens*: cell-bound fine-grained minerals are not always formed de novo. *Appl. Environ. Microbiol.* 67, 5544–5550.
- Glasauer, S., Weidler, P.G., Langley, S., Beveridge, T.J., 2003. Controls on Fe reduction and mineral formation by a subsurface bacterium. *Geochim. Cosmochim. Acta* 67, 1277–1288.
- Haas, J.R., DiChristina, T.J., 2002. Effects of Fe(III) chemical speciation on dissimilatory Fe(III) reduction by *Shewanella putrefaciens*. *Environ. Sci. Technol.* 36, 373–380.
- Hansley, P.L., Spirakis, C.S., 1992. Organic-matter diagenesis as the key to a unifying theory for the genesis of tabular uranium-vanadium deposits in the Morrison Formation, Colorado Plateau. *Econ. Geol.* 87, 352–365.
- Hao, L., Zhang, B., Feng, C., Zhang, Z., Lei, Z., Shimizu, K., Xuelong, C., Liu, H., Liu, H., 2018. Microbial vanadium (V) reduction in groundwater with different soils from vanadium ore mining areas. *Chemosphere* 202, 272–279.
- Hitchcock, A., 2019. An IDL-Based Analytical Package. <http://unicorn.mcmaster.ca>.
- Hostetler, P.B., Garrels, R.M., 1962. Transportation and precipitation of uranium and vanadium at low temperatures with special reference to sandstone-type uranium deposits. *Econ. Geol.* 57, 137–167.
- Huang, J.H., Huang, F., Evans, L., Glasauer, S., 2015. Vanadium: Global (bio) geochemistry. *Chem. Geol.* 417, 68–89.
- Hunter, R.C., Beveridge, T.J., 2005. Application of a pH-sensitive fluorophore (C-SNARF-4) for pH microenvironment analysis in *Pseudomonas aeruginosa* biofilms. (2005) *Appl. Environ. Microbiol.* 71, 2501–2510.

- Ilangovan, U., Ton-That, H., Iwahara, J., Schneewind, O., Clubb, R.T., 2001. Structure of sortase, the transpeptidase that anchors proteins to the cell wall of *Staphylococcus aureus*. *Proc. Natl. Acad. Sci.* 98, 6056–6061.
- Iltou, E.S., Liu, C., Yantasee, W., Wang, Z., Moore, D.A., Felmy, A.R., Zachara, J.M., 2006. The dissolution of synthetic Na-boltwoodite in sodium carbonate solutions. *Geochim. Cosmochim. Acta* 70, 4836–4849.
- Kalkowski, G., Kaindl, G., Brewer, W.D., Krone, W., 1987. Near edge X-ray absorption fine structure in uranium minerals. *Phys. Rev. B* 35, 2667–2677.
- Khijniak, T.V., Slobodkin, A., Coker, V., Renshaw, J.C., Livens, F.R., Bonch-Osmolovskaya, E.A., Birkeland, N.K., Medvedeva-Lyalikova, N.N., Lloyd, J.R., 2005. Reduction of uranium (VI) phosphate during growth of the thermophilic bacterium *Thermoterrabacterium ferrireducens*. *Appl. Environ. Microbiol.* 71, 6423–6426.
- Kolhe, N., Zinjarde, S., Acharya, C., 2018. Responses exhibited by various microbial groups relevant to uranium exposure. *Biotechnol. Adv.* 36, 1828–1846.
- Langmuir, D., 1978. Uranium solution-mineral equilibria at low temperatures with applications to sedimentary ore deposits. *Geochim. Cosmochim. Acta* 42, 547–569.
- Le Bail, A., Duroy, H., Fourquet, J., 1988. Ab-initio structure determination of LiSbWO_6 by X-ray powder diffraction. *Math. Res. Bull.* 23, 447–452.
- Lee, J.D., 1992. *Concise Inorganic Chemistry*, 4th ed. Chapman and Hall, London.
- Li, X.S., Glasauer, S., Le, X.C., 2007. Speciation of vanadium in oil sand coke and bacterial culture by high performance liquid chromatography inductively coupled plasma mass spectrometry. *Anal. Chim. Acta* 602, 17–22 and 648: 128 (2009).
- Li, L., Steefel, C.I., Kowalsky, M.B., Englert, Hubbard, S.S., 2010. Effects of physical and geochemical heterogeneities on mineral transformation and biomass accumulation during biostimulation experiments at Rifle, Colorado. *J. Contam. Hydrol.* 112, 45–63.
- Liu, C., Byong-Hun, J., Zachara, J.M., Zheming, W., Dohnalkova, A., Fredrickson, J.K., 2006. Kinetics of microbial reduction of solid phase U(VI). *Environ. Sci. Technol.* 40, 6290–6296.
- Liu, C., Zachara, J.M., Zhong, L., Heald, S.M., Wang, Z., Byong-Hun, J., Fredrickson, J.K., 2009. Microbial reduction of intragrain U(VI) in contaminated sediment. *Environ. Sci. Technol.* 43, 4928–4933.
- Lloyd, J.R., Renshaw, J.C., 2005. Bioremediation of radioactive waste: radionuclide-microbe interactions in laboratory and field-scale studies. *Curr. Opin. Biotechnol.* 16, 254–260.
- Lloyd, J.R., Chesnes, J., Glasauer, S., Bunker, D.J., Livens, F.R., Lovley, D.R., 2002. Reduction of actinides and fission products by Fe(III)-reducing bacteria. *Geomicrobiol J.* 19, 103–120.
- Lovley, D.R., Phillips, E.J.P., Gorby, Y.A., Landa, E.R., 1991. Microbial reduction of uranium. *Nature* 350, 413–416.
- Lyalikova, N.N., Yurkova, N.A., 1992. Role of microorganisms in vanadium concentration and dispersion. *Geomicrobiol J.* 10, 15–26.
- Macara, I.G., 1980. Vanadium – an element in search of a role. *Trends Biochem. Sci.* 5, 92–94.
- Maganas, D., Moemelt, M., Weyhermuller, T., Blume, R., Havecker, M., Knop-Gericke, A., DeBeer, S., Schlögl, R., Neese, F., 2014. L-edge X-ray absorption study of mononuclear vanadium complexes and spectral predictions using a restricted open shell configuration interaction ansatz. *Phys. Chem. Chem. Phys.* 16, 264–276.
- Minasian, S.G., Keith, J.M., Batista, E.R., Boland, K.S., Bradley, J.A., Daly, S.R., Sokaras, D., Kozimor, S.A., Lukens, W.W., Martin, R.L., Nordlund, D., Seidler, G.T., Shuh, D.K., Tyliczszak, T., Wagner, G., Weng, T.-C., Yang, P., 2013. (2013) Covalency in metal-oxygen multiple bonds evaluated K-edge spectroscopy and electronic structure theory. *J. Amer. Chem. Soc.* 135, 1864–1871. <https://doi.org/10.1021/ja310223b>.
- Myers, C.R., Myers, J.M., 1992. Localization of cytochromes to the outer membrane of anaerobically grown *Shewanella putrefaciens* MR-1. *J. Bacteriol.* 174, 3429–3438.
- Myszka, K., Czaczky, K., 2009. Characterization of adhesive exopolysaccharide (EPS) produced by *Pseudomonas aeruginosa* under starvation conditions. *Curr. Microbiol.* 58, 541–546.
- Naik, M.T., Suree, N., Ilangovan, U., Liew, C.K., Thieu, W., Campbell, D.O., Clemens, J.J., Jung, M.E., Clubb, R.T., 2006. *Staphylococcus aureus* Sortase A transpeptidase – Calcium promotes sorting signal binding by altering the mobility and structure of an active site loop. *J. Biol. Chem.* 281, 1817–1826.
- Nies, D.H., 2007. Bacterial transition metal homeostasis. In *Molecular Microbiology of Heavy Metals*, DH Nies and S Silver (eds). *Microbiol. Monogr.* 6, 117–142.
- Nilsson, H.J., Tyliczszak, T., Wilson, R.E., Werme, L., 2005. Shuh DK (2005) Soft X-ray scanning transmission X-ray microscopy (STXM) of actinide particles. *J. Anal. Bioanal. Chem.* 383, 41–47. <https://doi.org/10.1007/s00216-005-3355-5>.
- Ortiz-Bernad, I., Anderson, R.T., Vrionis, H.A., Lovley, D.R., 2004a. Vanadium respiration by *Geobacter metallireducens*: Novel strategy for in situ removal of vanadium from groundwater. *Appl. Environ. Microbiol.* 70, 3091–3095.
- Ortiz-Bernad, I., Anderson, R.T., Vrionis, H.A., Lovley, D.R., 2004b. Resistance of solid-phase U(VI) to microbial reduction during *in situ* bioremediation of uranium-contaminated groundwater. *Appl. Environ. Microbiol.* 70, 7558–7560.
- Premovic, P.I., Pavlovic, M.S., Pavlovic, N.Z., 1986. Vanadium in ancient sedimentary rock of marine origin. *Geochim. Cosmochim. Acta* 50, 1923–1931.
- Rehder, D., 2008. *Bioinorganic Vanadium Chemistry*. John Wiley & Sons, Chichester.
- Smeaton, C.M., Weisener, C.G., Burns, P.C., Fryer, B.J., Fowle, D.A., 2008. Bacterially enhanced dissolution of meta-autunite. *Am. Mineral.* 93, 1858–1864.
- Spirakis, C.S., 1996. The roles of organic matter in the formation of uranium deposits in sedimentary rocks. *Ore Geol. Rev.* 11, 53–69.
- Stern, T.W., Stieff, L.R., Girhard, M.N., Meyrowitz, R., 1956. The occurrence and properties of meta-tyuyamunite, $\text{Ca}(\text{UO}_2)_2(\text{VO}_4)_2 \cdot 3\text{H}_2\text{O}$. *Am. Mineral.* 41, 187–201.
- Stohl, F.V., Smith, D.K., 1981. The crystal chemistry of the uranyl silicate minerals. *Am. Mineral.* 66, 610–625.
- Stylo, M., Alessi, D.S., Shao, P.P., Lezama-Pacheco, J.S., Bargar, J.R., Bernier-Latmani, R., 2013. Biogeochemical controls on the product of microbial U(VI) reduction. *Environ. Sci. Technol.* 47, 12351–12358.
- Thews, K.B., Heinle, F.J., 1923. Extraction and recovery of radium, vanadium and uranium from carnotite. *Ind. Eng. Chem.* 15, 1159–1161.
- Tokunaga, T.K., Kim, Y., Wan, J.M., 2009. Potential remediation approach for uranium-contaminated groundwaters through potassium uranyl vanadate precipitation. *Environ. Sci. Technol.* 43, 5467–5471.
- Tokunaga, T.K., Kim, Y., Wan, J.M., Yang, L., 2012. Aqueous uranium (VI) concentrations controlled by calcium uranyl vanadate precipitates. *Environ. Sci. Technol.* 46, 7471–7477.
- Urrutia, M.M., Roden, E.E., Fredrickson, J.K., Zachara, J.M., 1998. Microbial and surface chemistry controls on reduction of synthetic Fe(III) oxide minerals by the dissimilatory iron-reducing bacterium *Shewanella* alga. *Geomicrobiol J.* 15, 269–291.
- Van der Laan, G., Moore, K.T., Tobin, J.G., Chung, B.W., Wall, M.A., Schwartz, A.J., 2004. *Phys. Rev. Lett.* 93, 097401.
- Vrionis, H.A., Anderson, R.T., Ortiz-Bernad, I., O'Neill, K.R., Resch, C.T., Peacock, A.D., Dayvault, R., White, D.C., Long, P.E., Lovley, D.R., 2005. Microbiological and geochemical heterogeneity in an *in situ* uranium bioremediation field site. *Appl. Environ. Microbiol.* 71, 6308–6318.
- Weeks, A.D., 1961. Mineralogy and geochemistry of vanadium in the Colorado Plateau. *J. Less-Common Metals* 3, 443–450.
- Wehrli, B., Stumm, W., 1989. Vanadyl in natural waters: Adsorption and hydrolysis promote oxygenation. *Geochim. Cosmochim. Acta* 53, 69–77.
- Wen, X.-D., Loble, M.W., Batista, E.R., Bauer, E., Boland, K.S., Burrell, A.K., Conradson, S.D., Daly, S.R., Kozimor, S.A., Minasian, S.G., Martin, R.L., McCleskey, T.M., Scott, B.L., Shuh, D.K., Tyliczszak, T., 2014. Electronic Structure and O K-edge XAS Spectroscopy of U_3O_8 . *J. Electron Spectrosc. Relat. Phenom.* 194, 81–87. <https://doi.org/10.1016/j.elecspec.2014.03.005>.
- Wiegand, I., Hilpert, K., Hancock, R.E.W., 2008. Agar and broth dilution methods to determine the minimum inhibitory concentration (MIC) of antimicrobial substances. *Nat. Protoc.* 3 (2), 163–175.
- Williams, K.H., Long, P.E., Davis, J.A., Wilkins, M.J., N'Guessan, A.L., Steefel, C.I., Yang, L., Newcomer, D., Spane, F.A., Kerkhof, L.J., McGuinness, L., Dayvault, R., Lovley, D.R., 2011. Acetate availability and its influence on sustainable bioremediation of uranium-contaminated groundwater. *Geomicrobiol J.* 28 (5–6), 519–539.
- Wu, Z.Y., Jollet, F., Gota, S., Thromat, N., Gautier-Soyer, M., Petit, T., 1999. X-ray absorption at the oxygen K edge in cubic f oxides examined using a full multiple-scattering approach. *J. Phys. Condens. Matter* 11, 7185–7194.
- Xu, J., Veeramani, H., Qafoku, N.P., Singh, G., Riquelme, M.V., Pruden, A., Kukkadapu, R.K., Gartman, B.N., Hochella, M.F., 2017. Efficacy of acetate-amended biostimulation for uranium sequestration: combined analysis of sediment/groundwater geochemistry and bacterial community structure. *Appl. Geochem.* 78, 172–185.
- Yang, U., Sakers, J.E., Xu, N., Minasian, S.G., Tyliczszak, T., Kozimor, S.A., Shuh, D.K., Barnett, M.O., 2012. Impact of natural organic matter on uranium transport through saturated geologic materials: from molecular to column scale. *Environ. Sci. Technol.* 46, 5931–5938.
- Yang, Y., Wang, S., Albrecht-Schmitt, T.E., 2014. Microbial dissolution and reduction of uranyl crystals by *Shewanella oneidensis* MR-1. *Chem. Geol.* 387, 59–65.
- Zachara, J.M., Fredrickson, J.K., Li, S.M., Kennedy, D.W., Smith, S.C., Gassman, P.L., 1998. Bacterial reduction of crystalline Fe^{3+} oxides in single phase suspensions and subsurface materials. *Am. Mineral.* 83, 1426–1443.
- Zhuang, K., Ma, E., Lovley, D.R., Mahadevan, R., 2012. The design of long-term effective uranium bioremediation strategy using a community metabolic model. *Biotechnol. Bioeng.* 109, 2475–2483.

Repository KITopen

Dies ist ein Postprint/begutachtetes Manuskript.

Empfohlene Zitierung:

Glasauer, S.; Fakra, S. C.; Schooling, S.; Weidler, P.; Tyliszczak, T.; Shuh, D. K.
[The transformation of U\(VI\) and V\(V\) in carnotite group minerals during dissimilatory respiration by a metal reducing bacterium.](#)
2022. Chemical Geology, 591.
doi:[10.5445/IR/1000146758](#)

Zitierung der Originalveröffentlichung:

Glasauer, S.; Fakra, S. C.; Schooling, S.; Weidler, P.; Tyliszczak, T.; Shuh, D. K.
[The transformation of U\(VI\) and V\(V\) in carnotite group minerals during dissimilatory respiration by a metal reducing bacterium.](#)
2022. Chemical Geology, 591, Art. Nr.: 120726.
doi:[10.1016/j.chemgeo.2022.120726](#)

Lizenzinformationen: [CC BY-NC-ND](#)